Materials & Design 235 (2023) 112408

Contents lists available at ScienceDirect

Materials & Design

journal homepage: www.elsevier.com/locate/matdes

An autonomous biodegradable hygroscopic seed-inspired soft robot for visual humidity sensing

Stefano Mariani [a,*], Luca Cecchini [a,b], Nicola M. Pugno [b,c], Barbara Mazzolai [a,*]

[a] Bioinspired Soft Robotics Laboratory, Istituto Italiano di Tecnologia, Via Morego 30, Genova 16163, Italy
[b] Laboratory for Bioinspired, Bionic, Nano, Meta Materials and Mechanics, Department of Civil, Environmental and Mechanical Engineering, University di Trento, Via Mesiano 77, Trento 38123, Italy
[c] School of Engineering and Materials Science, Queen Mary University of London, Mile End Road, London E1 4NS, UK

ARTICLE INFO

Keywords:
Visual humidity sensor
Environmental sensor
Hygro-mechanic effect
Bioinspired soft robotics
Artificial seeds
Geraniaceae seeds
Hygroscopic materials
Biodegradable materials
Additive manufacturing

ABSTRACT

Visual sensors for relative humidity (RH) are of interest for distributed and autonomous environmental monitoring. Most of the visual humidity sensors are based on colorimetric sensing through the employment of hygroscopic inorganic pigments or photonic crystals (PCs). However, the toxicity of some inorganic pigments poses a risk to the environment especially if dispersed during in-situ measurements. On the other hand, the angle-dependent structural colours reading of the PCs, make these devices non suitable for autonomous and in-situ environmental monitoring.

Here, we report the first visual humidity sensor using an artificial and hygroscopic seed-like robot (*I-SeedPel*) recently (2023) developed by our group for hygro-driven environmental exploration (https://doi.org/10.1002/advs.202205146).

The *I-SeedPel* design is bioinspired to the hygroscopic and layered tissues of the *Pelargonium appendiculatum* seed and fabricated through additive manufacturing techniques using biodegradable polymers. The hygro-mechanical response of the *I-SeedPel* generates a reversible change of the geometrical features in the artificial seed structure (i.e., awn's angular displacement and diameter variation) related to the RH. The variation of the geometric properties can be quantified and correlated to RH in a wide range (30–90 %), with an accuracy of 97–98 %, with a resolution of 0.17–0.52 % of RH and a good reproducibility (average RSD = 14.7 %).

1. Introduction

The measurement and control of relative humidity (RH) in air is essential for many applications in agriculture, in environmental monitoring, in biomedical technologies, in food industry [1] or in maintaining comfort building [2].

Electronic humidity sensors, based on various sensing mechanisms (i.e., amperometry or potentiometry, capacitive or resistive) are the most dominant in the market and in scientific literature [3–7]. However, there is still a need to search for other low cost, highly stable and visually readable colorimetric/optical sensors, which require no specific apparatus for operation, no battery onboard and that can be autonomously used in a wide range of areas (especially in remote area) [1].

Among the visually readable humidity sensors, the most common types involve commercial inorganic pigments-based Humidity Indicator Cards (HICs) or humidity responsive photonic crystals (PCs) [8].

In the case of commercial inorganic pigments (e.g., Cobalt chloride, $CoCl_2$), the hygroscopic inorganic salts absorb water from the environment once the RH increase, changing their reflected wavelength in the visible spectrum. For example, anhydrous cobalt chloride ($CoCl_2$) shows a pink colour, and after hydration due to the increase of RH, becomes cobalt chloride hexahydrate ($CoCl_2{\cdot}6H_2O$), changing its reflected colour in blue [9]. In the commercial HICs available in the market, the moisture sensitive spots are made of blotting cards impregnated with $CoCl_2$ that change colours in relation to the RH content.

However, $CoCl_2$ is a toxic chemical compound and classified by the European Union as category 2 i.e., carcinogen (Council Directive 67/548/EEC). In the Commission Directive 2004/73/EC (Apr. 29, 2004), $CoCl_2$ was also listed as a chemical substance which may cause cancer by inhalation at concentration of 0.01 % or higher. For the above-mentioned reasons, the use of $CoCl_2$ in industrial and commercial applications requires accurate control to ensure minimum exposure to the

* Corresponding authors.
E-mail addresses: stefano.mariani@iit.it (S. Mariani), barbara.mazzolai@iit.it (B. Mazzolai).

https://doi.org/10.1016/j.matdes.2023.112408
Received 24 July 2023; Received in revised form 2 October 2023; Accepted 15 October 2023
Available online 18 October 2023

humans and to the environment [10].

Consequently, several attempts have been made to find alternative materials to replace $CoCl_2$. New humidity-indicating medium and new cobalt-free HICs have been developed by some companies based on Copper Chloride ($CuCl_2$) [10]. However, also $CuCl_2$ is not an optimal alternative because of potential toxicity to the environment specially to aquatic life with long lasting effects (H410) [10]. For the above-mentioned reasons, the previously reported inorganic pigments based HICs pose high risk for the environment in the case of distributed and environmental RH sensing especially if the sensors are dispersed in the measuring field and not recovered.

Alternatively, humidity responsive photonic crystals (PCs) are also attractive devices for visually and colorimetric readable detection of RH avoiding the complex processes of data collection and display [11]. PCs are highly ordered materials which are characterized by a periodical modulation of the refractive index. The grating structure permits to control light propagation by modulating lattice constant [12–14]. The use of humidity sensitive materials for the manufacturing of PCs permits to modulate the light reflection, due to the shrinking or expansion of the crystal lattice.

Previous researches showed both humidity-responsive inorganic oxides [11] or polymers [15] (also biodegradable), composed with cellulose nanocrystals (CNC) [3,16–18] incorporated in PC structures for colorimetric humidity sensing.

However, in a PC the structural and observed colour greatly changes when an observer reads the information at different observation angles [19]; this decreases the accuracy of information and make these devices not suitable for accurate on-field humidity measurement especially using Unmanned Aerial Vehicle (UAV).

We report, here, a novel approach for the visual sensing of the RH using a seed-inspired soft robot (*I-SeedPel*) recently developed (2023) by our research group for autonomous environmental exploration [20] and capable of providing a hygro-mechanical variation of the geometrical structure and properties as a function of the RH content in the air. The RH sensor works autonomously powered by solely the RH variation itself.

The *I-SeedPel* is a soft robot bioinspired to *Pelargonium appendiculaum* seed, which belongs to the Gerianaceae family [21] and it combines explosive dispersal strategy with a hygroscopic autonomous motion on soil surface aimed to the penetration into soil fractures and germination. Crawling and burying occur thanks to the hygroscopic seed helical unit (the awn) that responds to variations of external humidity by changing its configuration thanks to hygroscopic cellulose-based microfibrils [21]. The *I-SeedPel* was fabricated through 4D printing additive manufacturing (FDM printing combined with coaxial electrospinning) using biodegradable polymers, namely polycaprolactone (PCL) [22], polyethylene oxide (PEO) [23] and cellulose nanocrystals (CNC) [24].

PCL was chosen as inactive and biodegradable thermoplastic materials for the good 3D printability and the good biodegradation rate (50 % weight loss in 300 days) [22]. In addition, compared to other common 3D printable biodegradable materials (e.g., Polylactic Acid, PLA), PCL is elastic and not-brittle [25]. These mechanical properties are fundamental for the development of the shape-changing *I-SeedPel* humidity sensor. PEO and CNC as biodegradable materials for the electrospinning were chosen considering the good processability [26,27]. In the coaxial electrospinning approach, used in this research, the CNC included in the PEO shell acts as reinforced stiffness material while the PEO shell is the hygroscopic adsorber [20].

Here, an alternative and smart employment of the *I-SeedPel* as humidity sensor is proposed by camera-capturing, correlation, and quantification of the geometric and configuration changes with the RH content of the air. To the best of our knowledge this is the first example of a green hygro-mechanical humidity sensor bioinspired to a seed and made entirely with biodegradable polymers.

The sensor provides two linear responses in a wide RH range (30–60 % and 60–90 %), an accuracy of 97–98 %, a resolution of 0.17–0.52 % RH and a good reproducibility (average RSD = 14.7 %).

In perspective, the *I-SeedPel* humidity sensor could be used for RH environmental monitoring, combing recording strategies based on vision via camera-equipped drones. This could be a unique and smart solution for in-situ, wireless and electronic-free measurement of humidity, especially in remote areas, using a biodegradable device that does not need to be retrieval after its function and working period.

2. Experimental section

2.1. *Pelargonium appendiculatum* seed

Pelargonium appendiculatum seeds were purchased from Greenmarket di Barbone Valerio, Bergamo Italy. An extensive morphometric, histological, mechanical and kinematics characterization of the *Pelargonium appendiculatum* seed has been previously reported [20].

2.2. *Artificial seed (I-SeedPel) fabrication*

The artificial seed (*I-SeedPel*) was fabricated trough a bioinspired approach using additive manufacturing techniques and coupling fused deposition modeling (3D-Bioplotter, EnvisionTEC, Germany) of PCL (Mw 45 000 Da, Sigma Aldrich, US) and coaxial electrospinning (Linari RT Advanced, Linari Engineering srl, Italy) of CNC core and PEO shell. The substrate production was detailed in the sketch reported Fig. 1a and previously and extensively described [20].

In summary, the inactive *I-SeedPel* was 3D printed using the design reported in Fig. 1b on an aluminium foil and fixing the temperature of the printing plate at 40 °C (Fig. 1c). The temperature of the hot-melt extruder was instead kept at 150 °C. We used a cylindrical nozzle

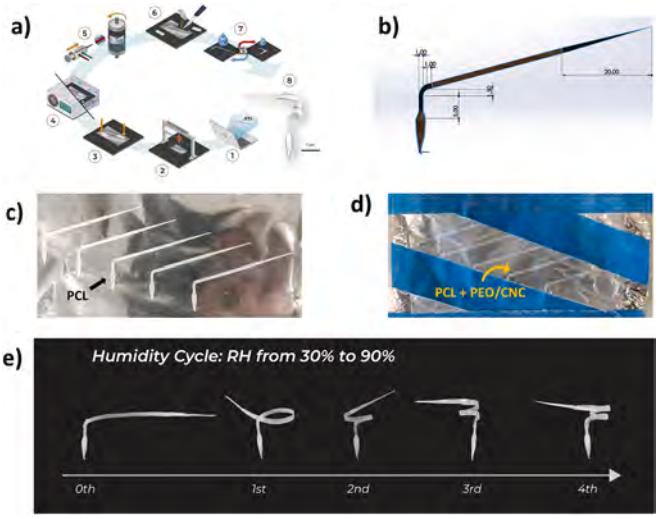

Fig. 1. a) Schematic representation of the printing process. (1) Design of the seed with CAD software for .stl production. (2) FDM printing of PCL on aluminum foil paper. (3) Adapting tape on artificial capsule and lever section. (4) Surface activation through oxygen plasma of the artificial awn. (5) Hygroscopic functionalization of the artificial awn through coaxial electrospinning of PEO/CNC. (6) Blade cut of the structure from aluminum-foil paper. (7) 4D deformation in a climatic chamber through 5-times humidity cycles. (8) Example of 4D printed artificial seed. Scalebar is 5 mm. **b)** Design of the lever, awn, and capsule of the *I-SeedPel*. **c)** FDM print of the PCL inactive layer of the *I-SeedPel* on an aluminum foil. **d)** The *I-SeedPel* were fixed on the aluminum foil using tape to prevent detachment during electrospinning process with PEO/CNC. e) Pictures of the deformation during consecutive humidity cycles for training of the *I-SeedPel* after the electrospinning process. Reproduced and adapted with permission. (Cecchini, L.; Mariani, S.; Ronzan, M.; Mondini, A.; Pugno, N. M.; Mazzolai, B. 4D Printing of Humidity-Driven Seed Inspired Soft Robots. *Adv. Sci.* **2023**, 2205146). Copyright 2023, John Wiley and Sons (CC BY 4.0 DEED).

(0.2 mm internal diameter and length 3 mm length). The extrusion pressure and the printing speed were set at 6 bar, and 11 mm/s, respectively. An air plasma treatment (Targeo Plasma Cleaner, PIE Scientific, US) was carried out to the PCL inactive surface using the following parameter: plasma power 150 W and time 30 s.

Then coaxial electrospinning on the air plasma-activated PCL surface was carried out with CNC core and PEO shell solutions (Fig. 1d). The CNC (Nanografi Nanotechnology AS, Turkey) solution was prepared at 5 % w/v. PEO (Mw 300 000 Da, Sigma Aldrich, US) solution was prepared at 10 % w/v, adding 5 % v/v of ethanol. Both were solubilized in deionized water and coaxially electrospun. The electrospinning conditions were set as follow: vertical speed of the syringe 1 cm/s, voltage 20 kV, drum rotation 2500 rpm; flow rate of the PEO shell solution 2 ml/h; flow rate of the CNC core solution 1 ml/h; RH = 20 %; T = 20 °C; round-trip cycles 250 (390 min) [20]. The electrospun *I-SeedPel* was then detached from the aluminium foil and trained with 4 consecutive humidity cycles 30–90 % for the trigger of the shape changing and hygroscopic activation (Fig. 1e).

2.3. Humidity sensing with natural Pelargonium appendiculatum and artificial seeds robot (I-SeedPel)

Humidity sensing measurements and calibration with the activated and hygroscopically-responsive *I-SeedPel* were carried out in a climatic chamber (CTC256, Memmert GmbH, Germany), fixing temperature T = 30 °C. The resolution and the accuracy set on the climatic chamber are 0.5 % and 1 %, respectively, as reported by datasheet of the CTC256 [28]. The choice of temperature value was chosen to guarantee the maximum humidity dynamics of the machine, that ranges from 30 % to 90 % with steps of 10 % every 10–20 min. Response times (Rt, s) and angular velocity (ω, °/s) were evaluated through the abrupt increase of humidity from 30 % to 90 % using a water aerosol.

Videos and pictures were acquired using Logitech Brio Stream, Logitech (Swiss), aligned to *Pelargonium appendiculatum* seed or *I-SeedPel* and placed at a distance at a distance of 10 cm. The Videos and picture were elaborated with Editor Video (Windows 10, Microsoft).

Digital measurement of the awns' angle displacements and of the awns' radius changes related to the humidity content in the air was carried out using ImageJ software [29].

3. Results and discussion

In the first step, we studied the applicability of the hygromechanic effect of the natural *Pelargonium appendiculatum* for visual humidity sensing purposes.

Hygroscopic movement in Gerianaceae seed involves coiling and decoiling based on a bi-layer construct in which one layer expand more than the other as it swells thank to the presence of cellulose-based microfibrils in cells, resulting in a coiling/uncoiling motion [20,21].

Fig. 2a shows the morphology of a *Pelargonium appendiculatum* seed consisting in: i) a capsule embedding the seed embryo; ii) the awn which is the helicoidal hygroscopic motor; iii) a lever, acting as passive element for the self-lifting of the seed and anchoring.

The camera position was selected to be orthogonal to the central axis of the helicoidal awn to evaluate digitally the angular displacement of the lever at different RH values with ImageJ [29] (Fig. 2b-h). We monitored the differential angular displacement of the lever angle (θ, °) every RH steps equal to 10 %, or compared to the initial lever position at RH = 30 % ($\theta_{30,}$ °) testing spanning RH conditions (30–90 %). The response time (Rt expressed in s) and the angular velocity (ω, expressed in °/s) related to θ_{30} were also monitored.

The collected data were summarized in Table S1, Supporting Information and in Fig. 2i, j.

Fig. 2i shows a progressive increase in angular displacement as the RH increases. Compared to the initial lever position for RH = 30 % the angular displacement θ_{30} (°) vs RH (%) could be fitted with a linear function $\theta_{30}(°) = 38.1RH(\%) - 1334(°)$ ($R^2 = 0.985$) (Fig. 2j). In first approximation, the data extracted from the geometrical characterization of the seed over different RH values proved that the geometrical parameter changes (i.e., awn's lever angular displacements) due to the hygro-mechanical response of *Pelargonium appendiculatum* could be visually quantified and correlated for visual humidity sensing purposes. Video S1, Supporting Information shows the angular displacement of the awn lever for a RH changing from 30 % to 90 %.

The response times (Rt, s) and angular velocity to RH variation (ω, °/s) from 30 % to 90 % RH were also evaluated accordingly to the procedure reported in Experimental Section. The Rt was 207 s and the calculated angular velocity was 10.6°/s. After assessed the suitability of the natural *Pelargonium appendiculatum* seed as a visual humidity sensor, we tested the performance of the *I-SeedPel* artificial seed (with statistical validation) using the previously reported setup and experimental methodology.

Recently (2023), we have reported the 4D printing of a soft seed-like robots based on hygroscopic biodegradable bilayer composite inspired by *Pelargonium appendiculatum* seed, both in the design and material arrangement. The artificial seed was conceived for explore the soil passively, driven by humidity changes, and penetrates fractures similarly to the natural ones, for environmental exploration and monitoring [20]. That research was the first attempt to develop soft robots truly bioinspired by seeds capable of hygroscopic actuation and autonomous passive motion on the soil. From a methodological point of view, the proposed research was based on an interdisciplinary approach consisting of: a) biological analysis of *Pelargonium appendiculatum* (i.e., histological, morphological, and structural analysis to extract the key parameters to implement onto the soft robot); b) design of the soft robot accordingly to the parameters extracted by the biological analysis; c) biomechanical analysis to predict and model the kinematic and deformation behaviours of natural and artificial seed as function of relative humidity variation; d) fabrication process of the artificial seed based on 4D printing of biodegradable polymers coupling Fused Deposition Melting (FDM) of PCL (hygroscopic-inactive material) with coaxial electrospinning of PEO and CNC core (hygroscopic active material). The whole *I-SeedPel* fabrication is reported in Fig. 1.

Similarly, to the *Pelargonium appendiculatum* natural seed, the developed artificial seed (*I-SeedPel*) was composed by a capsule that could enter inside soil fractures, a hygroscopic awn capable of coiling/uncoiling as a function of the humidity and a lever which functions as a passive element that allows the self-lifting (Fig. 3a).

In this research the awn's lever angular displacements (θ and θ_{30}), once inserted the capsule in a hole, were measured as a function of the humidity for humidity sensing. In addition, from a macroscopic point of view, the helical motion of the awn and the lever could be predicted considering the diameter of the awn (D). Also, D was measured and correlated to the humidity changes.

Fig. 3b-h and Video S2, Supporting Information reports the angular and diameter variation for the *I-SeedPel* as the RH increases from 30% to 90%.

The collected data are summerized in Table S2, Supplementary Information.

Considering the geometrical parameters that characterize the hygroscopic actuator (length, width, and thickness), the structure behaves like a laminate composite where only thickness participates in the deformation of the body. This hypothesis is valid if the thickness is sufficiently lower with respect to width and length (Kirchhoff assumption) [20]. Therefore, for the proposed design the variation of radius, pitch, and angles as function of RH are independent on width and length.

The achieved data confirmed that *I-SeedPel* could be used as visual humidity sensor considering the angular displacement θ_{30} at the different RH. The reproducibility expressed as average relative standard deviation (RSD) for θ_{30}, at the different humidity levels, was 14.8 % (N = 4). The trend could be fitted with exponential function ($R^2 = 0.981$, Fig. 4a). The exponential fitting (i.e., the increase of sensitivity with the

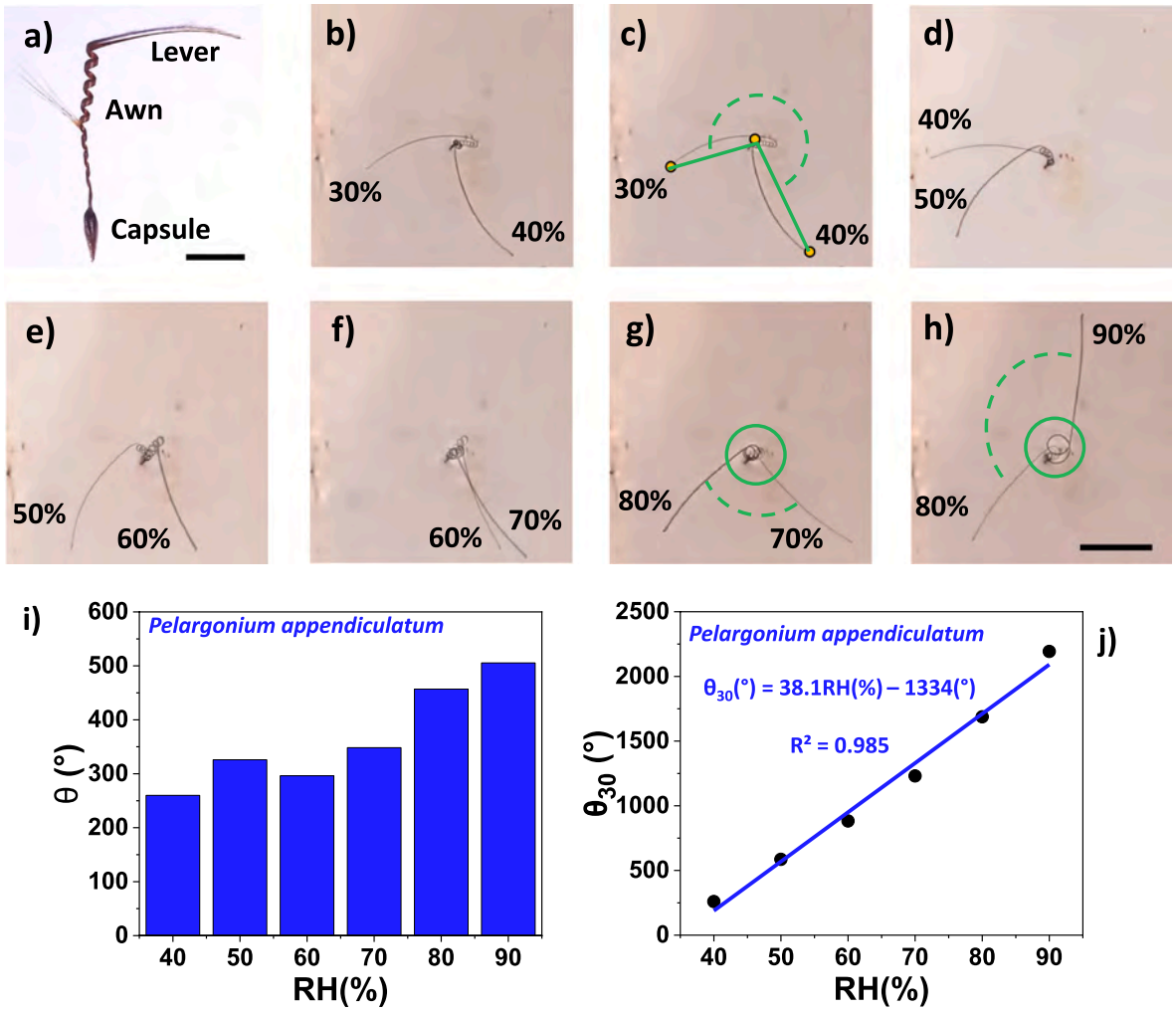

Fig. 2. a) Picture of a *Pelargonium appendiculatum* seed showing capsule, awn, and lever. Scalebar is 1 cm. **b)** Superimposed captured frame of the *Pelargonium appendiculatum* seed lever position at RH values of 30 % and 40 %. **c)** Angle displacement measurement of the lever rotation from RH 30–40 %. **d-h)** Superimposed frame of the *Pelargonium appendiculatum* seed lever rotation at different RH variations. **i)** Diagram showing Angle variation (θ) at different RH value for *Pelargonium appendiculatum* seed lever. **j)** Angle variations compared to RH = 30 % (θ_{30}) at different RH values for *Pelargonium appendiculatum* seed lever. The linear fitting function is also reported.

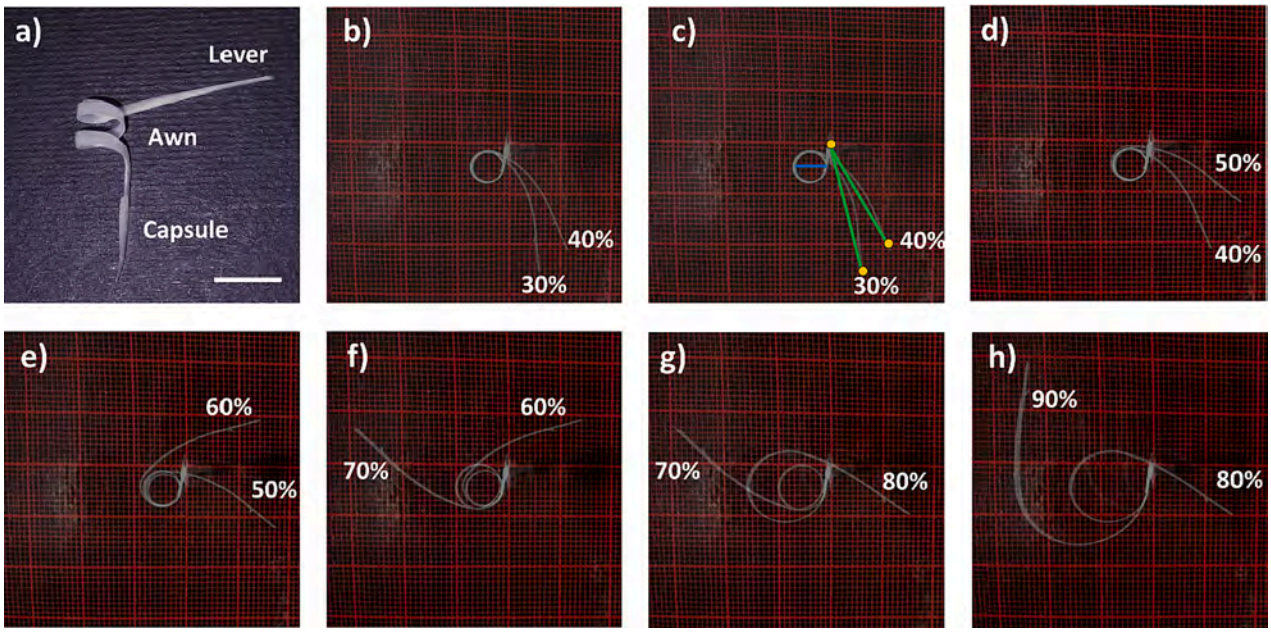

Fig. 3. a) Picture of a *I-SeedPel* showing capsule, awn, and lever. Scalebar is 1 cm. **b)** Superimposed frame of the *I-SeedPel* seed lever at RH values of 30 % and 40 %. **c)** Angle measurement of the lever displacement and diameter measurement reported in (b). **d-h)** Superimposed frame of the *I-SeedPel* seed lever rotation at different RH variations.

increase of the humidity) is in agreement with the decrease of the storage modulus of PEO fibers and coaxial PEO/CNC fibers of the I-SeedPel (hygroscopic section) with the increase of RH measured through tensile tests [20,30]. Alternatively, the trend can be fitted approximately with two linear functions (Fig. 4b) for perspective sensing applications: $\theta_{30}(^\circ) = 4.57RH(\%) - 164(^\circ)$ ($R^2 = 0.974$ (RH $\leq$ 60 %)) and $\theta_{30}(^\circ) = 13.8RH(\%) - 710(^\circ)$ ($R^2 = 0.982$, (RH $\geq$ 60 %)). From the two linear ranges we can also estimate two different sensitivities (°/%RH): 4.57°/%RH and 13.8°/%RH for the 30–60 % and RH 60–90 % ranges, respectively.

In addition, Table S3, Supporting Information shows also that the *I-SeedPel* could be used as visual humidity sensor monitoring and also measuring the D changes at different RH. The reproducibility expressed as average relative standard deviation for D at the different humidity levels was 5.8 % (N = 3). The trend can be fitted with exponential function, $D(mm) = 5.6(mm) + 0.0023e^{0.1RH(\%)}$ ($R^2 = 0.993$) (Fig. 4c) or alternatively with two linear functions $D(mm) = 0.066RH(\%) + 3.4$ (mm) ($R^2 = 0.952$ (RH $\leq$ 60 %) and $D(mm) = 0.87RH(\%) - 53.4(mm)$ ($R^2 = 0.999$ (RH $\geq$ 60 %) (Fig. 4d).

Rt (s) of the *I-SeedPel* showed an average value of 85.3 ± 9.3 s for the whole tested humidity ranges 30–90 %. The Rt was the 41.2 % of *Pelargonium appendiculatum* one. This result proved the *I-SeedPel* was faster in terms of Rt (i.e., more responsive) than the natural seeds (Fig. 4e).

The average angular velocity (°/s) of the *I-SeedPel* was 5.61 ± 1.67°/s and it was roughly the 53 % compared to the *Pelargonium appendiculatum* one (Fig. 4f).

We also estimated the resolution (R) of the *I-SeedPel* RH sensor in terms of %RH (Fig. 5a-d), considering the lower measurable lever angular displacement by our camera after a zoom of 2X (Fig. 5a, b) and 6X (Fig. 5c, d) and after a post-processing image analysis.

We defined the angular displacement θ_R resolved when the distance between the acquired levers (before and after the humidity changes) was equal to the thickness of the lever itself as shown in Fig. 5c, d. In Fig. 5d we have increased the contrast of the image to better show the resolved levers. A $\theta_R = 2.36^\circ$ was measured. Considering the two linear fitting reported in Fig. 4b two different humidity sensor resolutions R were calculated: 0.52 % and 0.17 % for the linear fitting with slope 4.57°/% (RH $\leq$ 60 %) and 13.8°/% (RH $\geq$ 60 %), respectively.

It is interesting to point out that R values achieved are much lower than those of colorimetric systems based on photonic crystals or interferometric films which range from 1.5 to 10 % [3]. In addition, we would like to stress that this type of sensor, made of biodegradable materials and battery-free has a resolution comparable to the DHT11 temperature and humidity digital sensor (1 %) [31].

All the reported performances confirmed the suitability of the *I-SeedPel* for the environmental RH measurements. At this purpose, as a simulation of a perspective real application case, we put the *I-SeedPel* on a model soil, testing RH variation from 30 % to 60 % and recording the θ_{30} angular displacement (Fig. 6a-c and Video S3, Supporting Information) and exploiting the linear relationships reported in Fig. 4b.

The measured θ_{30} was 103° and from the linear interpolations, the achieved RH values were 58.4 % and 58.9 % (Fig. 6d) resulting in a high accuracy of 97.3 % and 98.1, respectively. Alternatively, using the exponential interpolation reported in Fig. 4a ($\theta_{30}(^\circ) = -64(^\circ) + 16e^{0.04RH(\%)}$), the achieved RH value is 58.6 %, resulting in a similar accuracy of 97.7 %. These results confirmed the feasibility of using this autonomous green sensor, powered by humidity itself and made of biodegradable polymers, for humidity measurements on the field.

4. Conclusions

In summary, we proved that the hygro-mechanic effect of the hygroscopic natural Geraniaceae seeds (i.e., *Pelargonium appendiculatum*) promotes geometric variation of the structure (i.e., awn's lever angular displacement) that can be captured and correlated to the RH humidity changes in the air. This has prompted an application for humidity visual sensing.

At this purpose, a soft-robot bioinspired to *Pelargonium appendiculatum (I-SeedPel)*, recently (2023) developed by our group for hygro-driven environmental exploration (https://doi.org/10.1002/advs.202205146) [20] and made of biodegradable polymers, was tested for humidity sensing purpose, exploiting its hygro-mechanical effect, and relating the angular displacement and the diameter variation of the artificial awn with the RH variation (30–90 %).

The angular-based sensing has a good reproducibility (RSD = 14.8

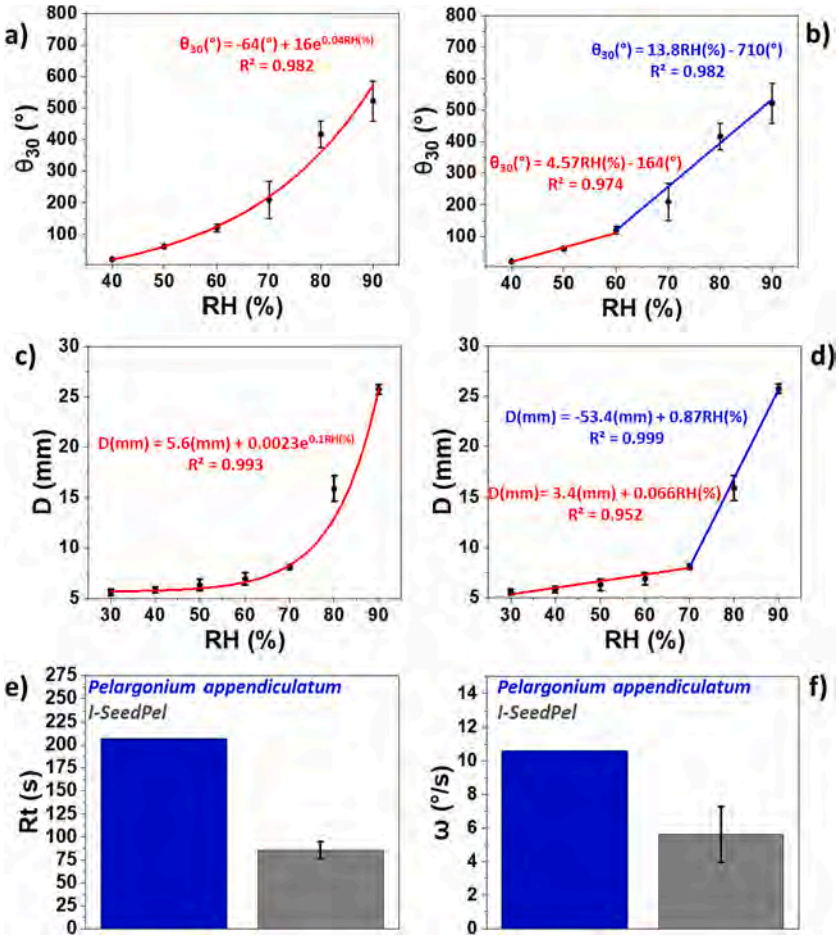

Fig. 4. **a)** Awn's lever angular displacement of the *I-SeedPel* at different RH values compared to RH = 30% (θ_{30}). The exponential fitting function is also reported. **b)** The same diagram of (a) with linear fittings is reported. **c)** Diagram showing diameter (D) variations at different RH values for *I-SeedPel*. Exponential fitting is also reported. **d)** The same diagram of (c) with linear fittings is reported. **e)** Response time (Rt, s) of the *Pelargonium appendiculatum* seed and *I-SeedPel* lever from 30-90% RH. **(f)** Angular velocity (ω, °/s) of the *Pelargonium appendiculatum* seed and *I-SeedPel* lever from 30-90% RH.

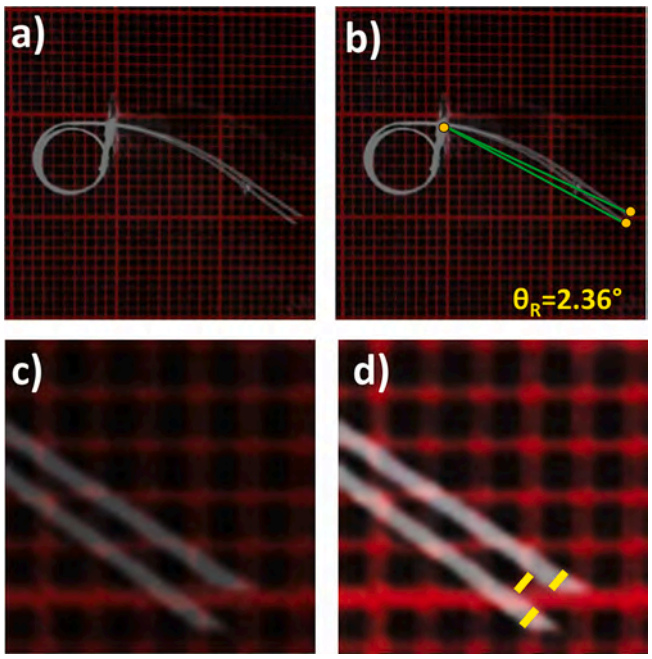

Fig. 5. **a)** Superimposed frame of the *I-SeedPel* seed lever for the estimation of the sensor resolution, through the estimation of the lower angular lever displacement recognizable θ_R. **b)** Angle measurement of the lever displacement of the figure reported in (a). **c)** Zoom (3X) of the lever extremity reported in a). **d)** Picture reported in (c) with enhanced contrast.

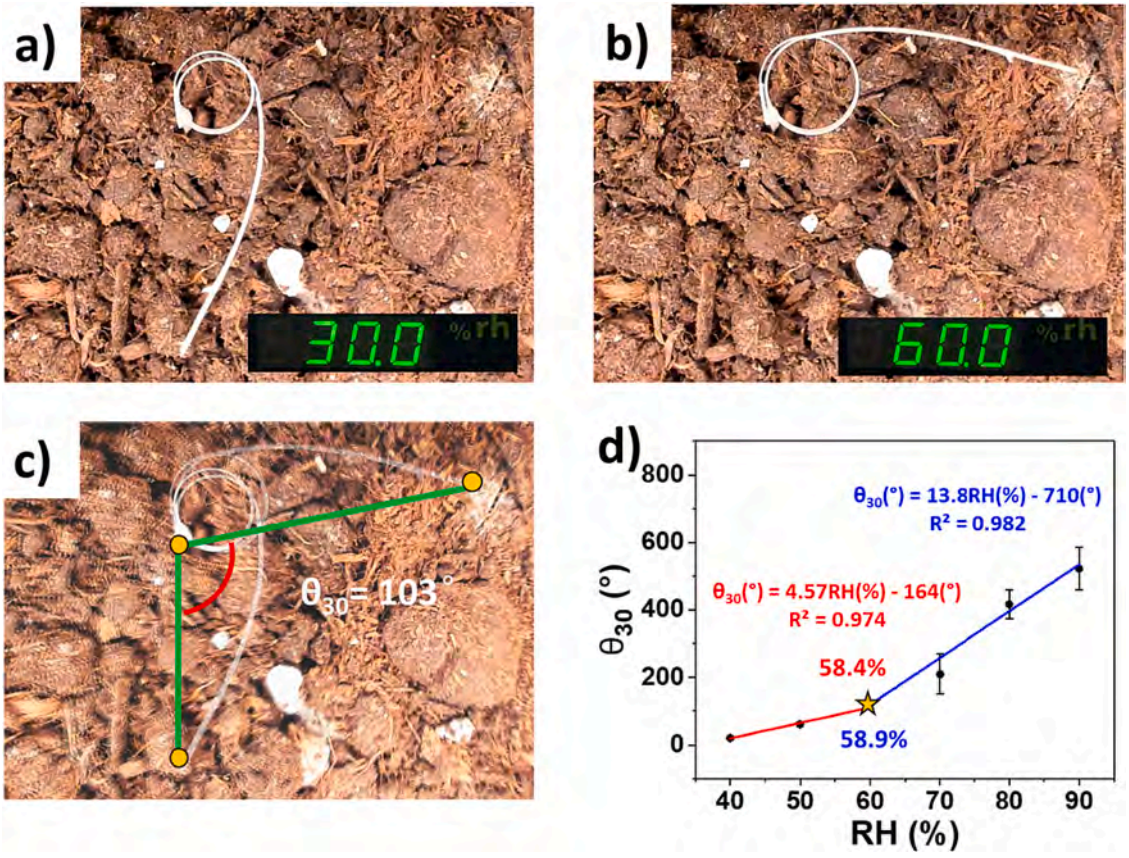

Fig. 6. **a)** Picture of the *I-SeedPel* lever at a RH value of 30% once the *I-SeedPel* is inserted in the ground. **b)** Picture of the *I-SeedPel* lever at a RH value of 60% once the *I-SeedPel* is inserted in the ground. **c)** Angle measurement of the lever angular displacement from RH = 30% (a) to RH = 60%. **d)** Interpolation of the RH(%) value considering the linear fitting reported in Fig. 4b, for the accuracy measurement evaluation.

%) and accuracy (97–98 %). The sensor has also a good resolution (i.e., 0.52 % and 0.17 % RH) better than photonic crystal-based humidity sensor, and comparable to some electronic digital sensors.

Although the measurement was characterized in a commercial humid chamber, it is easy to envision a distributed measurement with drones equipped with camera for acquisition and the evaluation of the angular awn's lever displacement and correlation to RH content in the air.

Thanks to the biodegradability of the employed polymers (i.e., PCL, CNC and PEO) in the soil, once the humidity sensors have performed their function it is not necessary to retrieve them.

The combination of in-situ measurement with remote monitoring (wireless), could pave the way to a new generation of RH sensor (powered by the RH variation itself) also for remote areas and/or with poor-resources.

Declaration of Competing Interest

The authors declare that they have no known competing financial interests or personal relationships that could have appeared to influence the work reported in this paper.

Data availability

Data will be made available on request.

Acknowledgments

This work has received funding from the European Union Horizon 2020 research and innovation programme under grant agreement no. 101017940 (I-Seed).

Appendix A. Supplementary data

Supplementary data to this article can be found online at https://doi.org/10.1016/j.matdes.2023.112408.

References

[1] V. Montes-García, P. Samorì, Humidity sensing with supramolecular nanostructures, Adv. Mater. (2023) 2208766, https://doi.org/10.1002/adma.202208766.
[2] H. Hu, Q.-W. Chen, K. Cheng, J. Tang, Visually readable and highly stable self-display photonic humidity sensor, J. Mater. Chem. 22 (2012) 1021–1027, https://doi.org/10.1039/C1JM14463D.
[3] M. Momtaz, J. Chen, High-performance colorimetric humidity sensors based on Konjac Glucomannan, ACS Appl. Mater. Interfaces 12 (2020) 54104–54116, https://doi.org/10.1021/acsami.0c16495.
[4] Z. Ahmad, F. Touati, Q. Zafar, M. Shah, Integrated Capacitive and Resistive Humidity Transduction via Surface Type Nickel Phthalocyanine Based Sensor, Int. J. Electrochem. Sci. 12 (2017) 3012–3019, https://doi.org/10.20964/2017.04.21.
[5] M.I. Azmer, Q. Zafar, K.W. Qadir, K. Sulaiman, T.M. Bawazeer, M.S. Alsoufi, Organic humidity sensing film optimization by embedding inorganic nano-anatase TiO2 powder, Appl. Phys. A 124 (2018) 508, https://doi.org/10.1007/s00339-018-1924-7.
[6] R. Akram, M. Yaseen, Z. Farooq, A. Rauf, Z.M. Almohaimeed, M. Ikram, Q. Zafar, Capacitive and Conductometric Type Dual-Mode Relative Humidity Sensor Based on 5,10,15,20-tetra Phenyl Porphyrinato Nickel (II) (TPPNi), Polymers (basel). 13 (2021), https://doi.org/10.3390/polym13193336.
[7] Q. Zafar, M.I. Azmer, A.G. Al-Sehemi, M.S. Al-Assiri, A. Kalam, K. Sulaiman, Evaluation of humidity sensing properties of TMBHPET thin film embedded with spinel cobalt ferrite nanoparticles, J. Nanoparticle Res. 18 (2016) 186, https://doi.org/10.1007/s11051-016-3488-9.
[8] X. Rao, L. Zhao, L. Xu, Y. Wang, K. Liu, Y. Wang, G.Y. Chen, T. Liu, Y. Wang, Review of Optical Humidity Sensors, Sensors 21 (2021), https://doi.org/10.3390/s21238049.
[9] Y. Kan, J. Meng, Y. Guo, X. Li, D. Gao, Humidity sensor based on cobalt Chloride/Cellulose Filter-Paper for respiration monitoring, J. Electroanal. Chem. 895 (2021), 115423, https://doi.org/10.1016/j.jelechem.2021.115423.
[10] https://patents.google.com/patent/US20050106735A1/en (Accessed 2023/06/04).
[11] D. Kou, W. Ma, S. Zhang, J.L. Lutkenhaus, B. Tang, High-Performance and Multifunctional Colorimetric Humidity Sensors Based on Mesoporous Photonic Crystals and Nanogels, ACS Appl. Mater. Interfaces 10 (2018) 41645–41654, https://doi.org/10.1021/acsami.8b14223.
[12] A.K. Yetisen, H. Butt, S.-H. Yun, Photonic Crystal Flakes, ACS Sens. 1 (2016) 493–497, https://doi.org/10.1021/acssensors.6b00108.
[13] S. Mariani, V. Robbiano, R. Iglio, A.A. La Mattina, P. Nadimi, J. Wang, B. Kim, T. Kumeria, M.J. Sailor, G. Barillaro, Moldless Printing of Silicone Lenses with Embedded Nanostructured Optical Filters, Adv. Funct. Mater. 30 (2020) 1906836, https://doi.org/10.1002/adfm.201906836.
[14] J. Chi, M. Su, B. Xue, L. Cheng, Z. Lian, Y. Yun, X. Yang, X. Wang, H. Xie, H. Wang, Y. Wang, J. Du, Y. Song, Fast and Sensitive Detection of Protein Markers Using an All-Printing Photonic Crystal Microarray via Fingertip Blood, ACS Sens. 8 (2023) 1742–1749, https://doi.org/10.1021/acssensors.3c00029.
[15] E. Tian, J. Wang, Y. Zheng, Y. Song, L. Jiang, D. Zhu, Colorful humidity sensitive photonic crystal hydrogel, J. Mater. Chem. 18 (2008) 1116–1122, https://doi.org/10.1039/B717368G.
[16] H. Chen, A. Hou, C. Zheng, J. Tang, K. Xie, A. Gao, Light- and Humidity-Responsive Chiral Nematic Photonic Crystal Films Based on Cellulose Nanocrystals, ACS Appl. Mater. Interfaces 12 (2020) 24505–24511, https://doi.org/10.1021/acsami.0c05139.
[17] K. Yao, Q. Meng, V. Bulone, Q. Zhou, Flexible and Responsive Chiral Nematic Cellulose Nanocrystal/Poly(ethylene glycol) Composite Films with Uniform and Tunable Structural Color, Adv. Mater. 29 (2017) 1701323, https://doi.org/10.1002/adma.201701323.
[18] M. Xu, W. Li, C. Ma, H. Yu, Y. Wu, Y. Wang, Z. Chen, J. Li, S. Liu, Multifunctional chiral nematic cellulose nanocrystals/glycerol structural colored nanocomposites for intelligent responsive films, photonic inks and iridescent coatings, J. Mater. Chem. C 6 (2018) 5391–5400, https://doi.org/10.1039/C8TC01321G.
[19] S. Wu, J. Nan, Y. Wu, Z. Meng, S. Zhang, Low-Angle-Dependent Anticounterfeiting Label Decoded by Alcohol Tissue Wiping Based on a Multilayer Photonic Crystal Structure, ACS Appl. Mater. Interfaces 14 (2022) 27048–27055, https://doi.org/10.1021/acsami.2c04901.
[20] L. Cecchini, S. Mariani, M. Ronzan, A. Mondini, N.M. Pugno, B. Mazzolai, 4D Printing of Humidity-Driven Seed Inspired Soft Robots, Adv. Sci. (2023) 2205146, https://doi.org/10.1002/advs.202205146.
[21] Y. Abraham, R. Elbaum, Hygroscopic movements in Geraniaceae: the structural variations that are responsible for coiling or bending, New Phytol. 199 (2013) 584–594, https://doi.org/10.1111/nph.12254.
[22] A.S. Al Hosni, J.K. Pittman, G.D. Robson, Microbial degradation of four biodegradable polymers in soil and compost demonstrating polycaprolactone as an ideal compostable plastic, Waste Manag. 97 (2019) 105–114, https://doi.org/10.1016/j.wasman.2019.07.042.
[23] D. Kai, S.S. Liow, X.J. Loh, Biodegradable polymers for electrospinning: Towards biomedical applications, Mater. Sci. Eng. C 45 (2014) 659–670, https://doi.org/10.1016/j.msec.2014.04.051.
[24] F.V. Ferreira, A. Dufresne, I.F. Pinheiro, D.H.S. Souza, R.F. Gouveia, L.H.I. Mei, L. M.F. Lona, How do cellulose nanocrystals affect the overall properties of biodegradable polymer nanocomposites: A comprehensive review, Eur. Polym. J. 108 (2018) 274–285, https://doi.org/10.1016/j.eurpolymj.2018.08.045.
[25] R. V.G., J. Wilson, L. V. Thomas, P.D. Nair,, Assessing the 3D Printability of an Elastomeric Poly(caprolactone-co-lactide) Copolymer as a Potential Material for 3D Printing Tracheal Scaffolds, ACS Omega 7 (2022) 7002–7011, https://doi.org/10.1021/acsomega.1c06679.
[26] J. Xue, T. Wu, Y. Dai, Y. Xia, Electrospinning and Electrospun Nanofibers: Methods, Materials, and Applications, Chem. Rev. 119 (2019) 5298–5415, https://doi.org/10.1021/acs.chemrev.8b00593.
[27] Y. Zhang, C. Zhang, Y. Wang, Recent progress in cellulose-based electrospun nanofibers as multifunctional materials, Nanoscale Adv. 3 (2021) 6040–6047, https://doi.org/10.1039/D1NA00508A.
[28] https://www.memmert.com/products/climate-chambers/environmental-test-chambers/ctc256/pdf/ (Accessed 2023/09/21).
[29] C.A. Schneider, W.S. Rasband, K.W. Eliceiri, NIH Image to ImageJ: 25 years of image analysis, Nat. Meth. 9 (2012) 671–675, https://doi.org/10.1038/nmeth.2089.
[30] D. Lunni, M. Cianchetti, C. Filippeschi, E. Sinibaldi, B. Mazzolai, Plant-Inspired Soft Bistable Structures Based on Hygroscopic Electrospun Nanofibers, Adv. Mater. Interfaces 7 (2020) 1901310, https://doi.org/10.1002/admi.201901310.
[31] https://makeradvisor.com/tools/dht11-temperature-humidity-sensor/ (Accessed 2023/09/21).

SUPPORTING INFORMATION

An Autonomous Biodegradable Hygroscopic Seed-Inspired Soft Robot for Visual Humidity Sensing

Stefano Mariani [1,*], Luca Cecchini [1,2], Nicola M. Pugno [2,3], and Barbara Mazzolai [1,*]

[1]*Bioinspired Soft Robotics Laboratory, Istituto Italiano di Tecnologia, Via Morego 30, Genova, 16163 Italy*

[2]*Laboratory for Bioinspired, Bionic, Nano, Meta Materials and Mechanics, Department of Civil, Environmental and Mechanical Engineering, University di Trento, Via Mesiano 77, Trento, 38123 Italy*

[3]*School of Engineering and Materials Science, Queen Mary University of London, Mile End Road, London, E1 4NS UK*

**Corresponding authors: stefano.mariani@iit.it; barbara.mazzolai@iit.it*

Table S1: Angle displacement (θ, °) and angle displacement compared to RH= 30% (θ_{30}, °) of the *Pelargonium appendiculatum* seed lever measurement.

Table S2: Angle displacement (θ, °) and angle displacement compared to RH= 30% (θ_{30}, °) of the *I-SeedPel* lever measurement.

Table S3: Diameter variation compared to RH= 30% (D, mm) of the *I-SeedPel* lever measurement.

Table S1. Angle displacement (θ, °), angle displacement compared to RH= 30% ($\theta_{30,}$°) of the *Pelargonium appendiculatum* seed lever at different humidity values (30-90%). The linear fitting function is also reported.

Specie	RH (%)	θ (°)	θ_{30} (°)	Fitting function
Pelargonium appendiculatum	30-40	260	260	$\theta_{30}(°) = 38.1RH(\%) - 1334(°)$ $R^2 = 0.985$
	40-50	326	586	
	50-60	296	882	
	60-70	348	1231	
	70-80	457	1688	
	80-90	505	2193	

Table S2. Angle displacement (θ, °) and angle displacement compared to RH= 30% (θ_{30}, °) of the *I-SeedPel* lever at different humidity values (30-90%). Data are reported with error bars (N sample= 4) and with relative standard deviation (RSD, %). Logistic and linear fitting functions are also reported.

Specie	RH_{30} (%)	θ ± s.d. (°)	RSD (%)	θ_{30} ± s.d. (°)	RSD (%)	Fitting function
I-SeedPel (Angle)	30-40	20.2 ± 3.8	18.8	20.2 ± 3.8	18.8	$\theta_{30}(°) = -64(°) + 16e^{0.04RH(\%)}$ $R^2 = 0.982$ $\theta_{30}(°) = 4.57RH(\%) - 164(°)$ $R^2 = 0.974$ (RH ≤ 60%) $\theta_{30}(°) = 13.8RH(\%) - 710(°)$ $R^2 = 0.982$ (RH ≥60%)
	40-50	4.2 ± 6.5	15.8	61.4 ± 5.4	8.8	
	50-60	58.9 ± 11.7	19.9	120 ± 12	10	
	60-70	89.1 ± 50.0	56.1	209 ± 59	28.2	
	70-80	207 ± 69	33.3	416 ± 42	10.1	
	80-90	105 ± 37	32.2	522 ± 66	12.6	

Table S3. Diameter (D) of the *I-SeedPel* at different humidity values (30-90%). Data are reported with error bars (N sample= 3) and with relative standard deviation (RSD, %). Exponential and linear fitting functions are also reported.

Specie	RH (%)	D± s.d. (mm)	RSD (%)	Fitting function
I-SeedPel (Diameter)	30	5.6 ± 0.3	5.3	$D(mm) = 5.6(mm) + 0.0023e^{0.1RH(\%)}$ $R^2 = 0.993$ $D(mm) = 0.066RH(\%) + 3.4(mm)$ $R^2 = 0.952$ (RH ≤ 60%) $D(mm) = 0.87RH(\%) – 53.4(mm)$ $R^2 = 0.999$ (RH ≥60%)
	40	5.8 ± 0.3	5.2	
	50	6.3 ± 0.6	9.5	
	60	6.9 ± 0.6	8.6	
	70	8.1 ± 0.2	2.4	
	80	15.9 ± 1.2	7.5	
	90	25.7 ± 0.5	1.8	